

# **Large scale production of multi-walled carbon nanotubes by fluidized bed catalytic chemical vapor deposition : a parametric study**

Aurore Morançais<sup>1,2</sup>, Brigitte Caussat<sup>2\*</sup>, Yolande Kihn<sup>3</sup>, Philippe Serp<sup>1\*</sup>, Philippe Kalck<sup>1</sup>,  
Dominique Plee,<sup>5</sup> Patrice Gaillard<sup>5</sup>, Daniel Bernard<sup>4</sup>

<sup>1</sup>*LCCFP/ENSIACET/INPT, 118 route de Narbonne, 31077 Toulouse Cedex 4, France*

<sup>2</sup>*LGC/ENSIACET/INPT, UMR CNRS 5503, 5 rue Paulin Talabot, BP1301, 31106 Toulouse Cedex 1, France*

<sup>3</sup>*CEMES, UPR CNRS 8011, 29 rue Jeanne Marvig, 31055 Toulouse, France*

<sup>4</sup>*ARKEMA, 4-8 cours Michelet, La Défense 10, F-92091, Paris La Défense Cedex, France*

<sup>5</sup>*ARKEMA LACQ RESEARCH CENTER, PO Box 34, 64170 Lacq, France*

\* To whom correspondence should be addressed: Phone: +33 562885700; fax: +33

562885600 (P. Serp), Phone: +33 534615252; fax: +33 534615253 (B. Caussat)

*E-mail addresses:* Philippe.Serp@ensiacet.fr, Brigitte.Caussat@ensiacet.fr

## **Abstract**

A parametric study investigating the impact of temperature, run duration, total pressure, and composition of the gaseous phase on the catalytic growth of multi-walled carbon nanotubes (MWNT) has been performed. MWNT have been produced very selectively on the multi gram scale by catalytic chemical vapor deposition from ethylene in a fluidized bed reactor. The kinetics of MWNT growth is fast and, with the catalyst used, no induction period has been observed. The kinetic law is positive order in ethylene concentration and the process is limited by internal diffusion in the porosity of the catalyst. The formation of MWNT in the macroporosity of the catalyst induces an explosion of the catalyst grains. Such a process, thanks to the absence of temperature gradient and to the efficient mixing of the grains allows a uniform and selective treatment of the catalyst powder leading to very high selectivity towards MWNT formation. High purity MWNT have been obtained after catalyst dissolution. Depending on the temperature of production, the specific surface area of this material ranged between 95 and 455 m<sup>2</sup>/g.

Keywords : A. Carbon nanotubes; B. Chemical vapor deposition, Catalyst support; D. Carbon yield, Surface areas

## 1. Introduction

Multi-walled carbon nanotubes (MWNT) are today expected to bring significant breakthroughs in different fields such as: i) engineering materials, as additives for polymers or coatings to enhanced electrical and electrostatic properties or tenacity, ii) energy, as components of super-capacitors, fuel cells or batteries, iii) electronics, catalysis, .... Besides the key questions of standardization, safety, impact on environment, which are specific to each nanomaterial, if we focus on the current worldwide MWNT market status, some hard points appeared such as high prices (100 to 5000 €/kg) and poor availability (around 100 T/year). Middle term industrial production is realistic provided an efficient production process exists. The large scale synthesis of this material by catalytic chemical vapor deposition (CCVD) is the subject of intensive research, and appears to be the most promising route due to potential cheapness of the MWNT produced and to high yield productivities. Pilot scale production reactors are already running for graphite nanofibers and the two kinds of CNT, namely MWNT and single wall carbon (SWNT), and companies such as Arkema [1], Bayer [2] or Thomas Swan [3] are already present on the CNT market.

The CCVD process for carbon nanotubes (CNT) growth can be performed either under homogeneous or heterogeneous conditions [4]. In the former case, vapors of an organometallic catalyst precursor are mixed with reactant gases within the CVD reactor, leading to CNT growing in the vapor phase from the metallic particles as they are formed. This method, often called “floating catalyst” presents several drawbacks connected mainly to the difficulty to prevent particles coalescence. When using heterogeneous catalysts, fixed bed reactors represent the most common technology. The efficiency of CNT growth in this process is limited severely by inhomogeneous gas-solid contact and temperature gradients. Fluidized bed (FB) reactors can also be used for performing this process, and installations

have been tested, mainly in France [5], China [6,7] and in the Netherlands [8]. In that case, a catalytic powder is put into contact with reactant gases in appropriate conditions of flow rate, pressure, and temperature so as to allow homogeneous and heterogeneous chemical reactions to occur, leading to the catalytic formation of the desired product. The gas solid contact is regulated so as to fluidize each particle in the reactive gas, thus ensuring a vigorous mixing of powders by the gas. The control of the fluidization quality is of major importance to operate in isothermal conditions and to obtain uniform materials. Although some studies have appeared in the open literature dealing with the preparation of carbon nanofibers [8,9], MWNT [5-7,10-13] or even SWNT [14-16] by FB-CCVD, in most of them, no experimental data confirms the presence of a fluidization regime.

We have successfully adapted a CCVD process to be used in a fluidized bed reactor, and in a previous paper [5], the main advantages of our FB-CCVD process have been emphasized : (i) experiments are fully reproducible, (ii) they lead to high carbon conversions, more often higher than 75% and to an excellent selectivity in MWNT (neither soot nor encapsulated catalytic particles have been detected), (iii) elutriation is negligible, indicating that MWNT remain anchored on the catalytic particles in the FB. In this work, we present the first parametric study associated to the FB-CCVD process for large scale MWNT production.

## **1. Experimental features**

### ***Operating conditions tested***

The experimental set up employed is schematically presented in Fig. 1.

### **Figure 1**

The fluidized bed reactor is entirely constructed from a 304L stainless steel; its dimensions are 5.3 cm internal diameter and 1 m height. The gas distributor is a stainless steel perforated plate covered with a stainless steel grid supplied with 50  $\mu\text{m}$  holes, and an electric furnace allows monitoring of the fluidized bed temperature via two thermocouples, one fixed on the outer reactor wall and the other placed in the FB, 3 cm above the distributor. Electronic grade ethylene, hydrogen and nitrogen gases (Air Liquide) are supplied to the bed through a mass flow meter for the former and by ball rotameters for the two others. A pressure sensor allows measuring the differential pressure drop between the bottom and the top parts of the reactor. After its exit out of the reactor, the gaseous effluents flow through a bag filter, to collect elutriated particles or fines that could be formed during the experiments.

Catalyst supports consist in mesoporous alumina ( $\text{Al}_2\text{O}_3$ ) particles, 110 microns in mean diameter, previously treated in another reactor, in order to obtain a 2.5%Fe/ $\text{Al}_2\text{O}_3$  w/w catalyst; more details concerning the catalyst preparation are available elsewhere [17].

Concerning the operating procedure, first a mass of 50 g of catalyst is introduced into the reactor corresponding to an initial fixed bed height of 1.8 cm (we will see later why such a low value has been employed). A constant flow rate of pure nitrogen and hydrogen fluidizes the bed during its heating, the initial fluidization ratio  $U/U_{\text{mf}}$ , (where  $U$  is the gas flow velocity and  $U_{\text{mf}}$  the minimum fluidization velocity) being most often fixed to about 1. As soon as the thermal regime is reached, the flow rate of nitrogen is lowered to a pre-calculated value and simultaneously ethylene is introduced into the bed to maintain constant the total flow rate. It is worth noting that during the synthesis of CNT,  $U_{\text{mf}}$  decreases with run duration, since the grain density sharply decreases; as a consequence, the fluidization ratio increases with run duration as it will be detailed below. This explains why the initial fluidization ratio has been fixed to a minimum value.

In a first set of experiments, the influence of run duration and temperature has been analyzed. Run duration was varied between 5 and 150 minutes for a mean bed temperature of 650°C, then bed temperature, measured at 3 cm above the distributor, was varied between 450°C and 750°C for a run duration fixed at 120 minutes. The nitrogen, hydrogen and ethylene flow rates used during these experiments are respectively equal to 685, 1200 and 405 standard cm<sup>3</sup>/min (sccm). These values correspond to the nominal gas flow rates leading to an initial fluidization ratio  $U/U_{mf}$  equal to 1. The exact operating conditions tested are given in Table 1.

In a second series of runs (see Table 2), the influence of the gaseous phase (total gas flow rate, total pressure and C<sub>2</sub>H<sub>4</sub>/H<sub>2</sub> ratio) has been studied. For all these experiments, the mean bed temperature at 3 cm above the distributor was fixed at 650°C. The initial fluidization ratio has been varied between 0.6 and 1.1, the total pressure between 1 and 1.3 Bar and the C<sub>2</sub>H<sub>4</sub>/H<sub>2</sub> ratio between 0.1 and 0.66. Run R14 is similar to runs R6 and R10 which has allowed ascertaining the reproducibility of our experiments.

## Tables 1 and 2

### *Process efficiency*

The process efficiency was characterized through the following parameters:

- (i) the weight of produced material during each run, and the resulting deposition rate,
- (ii) the carbon yield, corresponding to the percentage of deposited carbon in comparison with the introduced quantity,
- (iii) the evolution of bed temperature (3 cm upon the distributor) with time, and of the mean pressure drop between the bottom and the top parts of the reactor.

This latter parameter gives information about the fluidization quality of catalytic powders and composites (CNT + catalyst) powders.

After each run, the whole bed of composite particles was chemically treated in a sulfuric acid bath, in order to completely dissolve the alumina and most of the iron catalyst.

SEM observations were done using a field-enhanced electron microscope (Hitachi S-4500 I) and a LEO 435 microscope; TEM observations were also conducted with a Philips CM12 microscope (120 kV voltage) in order to detect the possible presence of undesired products (soot or encapsulated iron nanoparticles).

Thermo gravimetric analyses (TGA) were conducted so as to evaluate the amount of carbon deposited in each experiment and also the percentage of other forms of carbon. Those analyses were conducted under air in a Setaram apparatus with a  $10^{\circ}\text{C}\cdot\text{min}^{-1}$  ramp between 25 and  $1000^{\circ}\text{C}$  followed by an isotherm at that temperature for 30 minutes.

Nitrogen adsorption-desorption analyses were performed using a Micromeritics Asap 2010 equipment, so as to obtain the BET specific surface area and information concerning the porosity of powders before and after CNT formation. The pore size distribution in the mesoporosity range was determined from the adsorption and desorption branches using the BJH method. Before each measurement, samples have been kept in an oven at  $100^{\circ}\text{C}$  to limit adsorption phenomena and a degassing has been performed at  $200^{\circ}\text{C}$  during 2h30min.

The distribution of grain diameters was measured with a Mastersizer Sirocco 2000 laser granulometer.

### **3. Results**

The specific surface area of the catalyst particles is  $178\text{ m}^2/\text{g}$ , and the pore size distribution is given in Fig. 2. These powders present significant meso-porosity, but also some

micro-porosity. This information is important in particular concerning the study of the total pressure influence presented below. The reproducibility of experiments tested through the nominal conditions of runs R6, R10 and R14 was satisfactory regarding all process parameters and material features. Elutriation phenomena have been negligible for all experiments. Similarly, attrition, due to the use of an abrasive support that could produce the cutting up of MWNT from the support was not observed. This latter result is in contradiction with observations reported by Hernadi et al. when studying the catalytic growth of MWNT on Fe/SiO<sub>2</sub> catalysts in a low diameter fluidized bed. In this study, the authors mentioned some drawbacks such as the formation of soot, in addition to the cutting up of the silica support and to the breaking of the MWNT due to agitation [18].

## **Figure 2**

### **3.1 Influence of run duration**

The operating conditions tested correspond to runs R1 to R7 of Table 1. First, systematic TGA measurements associated to TEM analysis have confirmed that for these operating conditions, the selectivity of the process is excellent: neither soot nor encapsulated particles were detected. The pressure drop monitoring has shown that the bed remains conveniently fluidized till 120 min of run. Beyond 120 min, fluidization quality decreases, but no agglomeration phenomenon has been observed. The evolution of final carbon yield, fixed bed height, MWNT weight and formation rate with run duration are given in Fig. 3.

## **Figure 3**



We do not believe that the fact to observe low reaction rates in the very early stages of the reaction is connected with catalyst activation period but rather to a short residence time of the gas in the catalyst bed. After some minutes, the MWNT formation rate reaches a value of  $0.2 \text{ g}_{\text{NT}}/\text{g}_{\text{Fe}}/\text{min}$ . The carbon yield and the CNT formation rate reach a maximum between 45 and 75 min. The relatively low values obtained in terms of yield, 71%, and growth rate,  $0.23 \text{ g}_{\text{CNT}}/\text{g}_{\text{Fe}}/\text{min}$ , in comparison with our previous results [5] can be rationalized by the fact that the initial bed mass used in the present study is quite low. Indeed, the objective of the study was not to optimize carbon yields but rather to analyze the evolution with time of process parameters. The MWNT weight and the fixed bed height are both increasing with time. It is worth noting that the catalyst still presents a noticeable activity after 150 min of run.

A peculiar phenomenon linked to the catalytic growth of MWNT is the impressive evolution of the fixed bed height with time: starting from 1.8 cm, it reaches 18 cm after 15 min and 69 cm after 150 min. This phenomenon is due to the important evolution of the powder morphology induced by CNT growth. MWNT form three dimensional randomly oriented hanks in which alumina particles are embedded. The mean particles size increases from  $110 \text{ }\mu\text{m}$  for the original catalyst powder to  $225 \text{ }\mu\text{m}$  for the composite powder obtained after 120 min. The apparent density of this composite powder is equal to  $134 \text{ kg}/\text{m}^3$  after 15 min of run,  $88 \text{ kg}/\text{m}^3$  after 30 min and  $55\text{-}60 \text{ kg}/\text{m}^3$  beyond this run duration. Similar values have been reported by Qian et al. [7]. Let us recall that the apparent initial not packed density of alumina particles is around  $1500 \text{ kg}/\text{m}^3$ . In terms of fluidization and process controls, this marked evolution must be carefully considered since the minimum fluidization velocity is roughly divided by a factor 6 after 120 min of run; this implies that the fluidization ratio increases with run duration of this same factor. Contrarily to the density, the BET surface

areas of the original catalyst (178 m<sup>2</sup>/g) and of the composite powder (169 m<sup>2</sup>/g) are very similar.

Furthermore, samples corresponding to each of these runs have been heated in air till 800°C so as to burn the MWNT and to collect the support constituted of alumina and remaining iron. These residues have been analyzed by laser granulometry. The evolution of the mean particles diameter with run duration is given in Fig. 4. We must add that pure alumina powder was also heated till 800°C and analyzed by laser granulometry in order to check that no diameter evolution was produced by this annealing. It can be seen that MWNT formation leads to a sharp decrease in the alumina mean diameter after 30 min of run, this diameter remaining stable beyond 30 to 40 min. It can then be deduced that MWNT grow to some extent into the macro pores of the alumina grains and exert a mechanical pressure leading to an explosion of alumina particles. To confirm this, SEM analysis of particles produced during run R2 have been performed, as shown in Fig. 5. It appears that the alumina surface presents a lamellar structure characteristic of exploded grains; such structure does not exist on the initial alumina surface. MWNT can be clearly seen anchored on these lamellar structures. This explosion is certainly beneficial to the catalytic efficiency of the process, since it opens the internal porosity of alumina grains and increases the accessibility to iron nanoparticles. Such behavior of the catalyst powders reminds the polyethylene formation on supported catalysts, which is also associated with an explosion of the catalyst grains.

### **Figures 4 and 5**

These results indicate that some catalytic iron nanoparticles are present into the pores of the alumina grains and that they are active for MWNT formation. They also show that MWNT nucleation on “new” accessible catalytic nanoparticles occurs mainly between 0 and

30 to 40 min. of run. Beyond this period of time, nucleation becomes more difficult and growth phenomena prevail. It is likely that the nanoparticles present on the outer surface of the alumina grains, and then in the macro-pores are the first to be active. A diffusion limitation should exist that limits the activity of the catalytic sites present into the meso- and micro-pores. Moreover, the fact that the carbon yield and MWNT formation rate are maximum between 45 and 75 min means that an intense growth stage of already formed MWNT occurs during this period. After 75 min, a progressive deactivation of the catalytic nanoparticles seems to occur, explaining the decrease in carbon yield and MWNT formation rate.

TEM observations have shown that MWNT of 10-20 nm external diameters and of micrometric length exist as early as 5 min of run. No induction period was observed for this process and MWNT nucleation and growth phenomena are very fast. In particular, it can be deduced from some TEM micrographs that the growing rate of MWNT in the first minutes of the process could locally reach the value of 10  $\mu\text{m}/\text{min}$ . It is worth noting that the Fe/Al<sub>2</sub>O<sub>3</sub> catalyst used in this study is in the reduced state. The amount of MWNT increases with run duration, forming more and more hanks. Moreover, it seems that the CNT outer diameter does not change with time, remaining around 17 nm. However, several HREM observations have been performed which show a decrease in the internal diameter, and hence an increase in the number of walls from around 5 after 5 min to 15-20 after 150 min. These observations are consistent with a growth mechanism in which each additional wall (graphene layer) is formed inside the tube and not on the outer surface. Due to the presence of hanks, the measurement of MWNT length is very difficult to perform. However, we have estimated that it could range between 1  $\mu\text{m}$  and several micrometers. Although in the case of aligned nanotubes, a control of the MWNT length with CVD duration has been reported [19], we were not able to establish correlation between MWNT length and run duration.

### 3.2 Influence of temperature

The experimental conditions tested correspond to runs R8 to R12 of Table 1. First, no agglomeration phenomenon has occurred during these runs and pressure drop measurements have indicated that the bed was always conveniently fluidized.

The influence of temperature on carbon yield, final fixed bed height, MWNT weight and formation rate is presented in Fig. 6. Maximum values of carbon yield, formation rate and final fixed bed height were reached at 650°C. Below 650°C, the carbon yield is very low, explaining the very low fixed bed heights and carbon formation rates. Beyond 650°C, some parasitic phenomena occur, which are responsible for a partial deactivation of the catalyst, as it will be explained below. The bed apparent density of this composite powder is equal to 1140 kg/m<sup>3</sup> at 450°C, 58 kg/m<sup>3</sup> at 650°C and 200-250 kg/m<sup>3</sup> beyond 650°C. Such a pronounced evolution of powder morphology with temperature points out the importance of an isothermal regime for MWNT growth. Fig. 7 shows the morphology of the grains of composite powders produced at different temperatures. At 550°C, MWNT appeared as long extended hanks, at 750°C the hanks are more compact. This compactness could explain the strong reduction in the fixed bed height observed at this temperature.

#### Figures 6 and 7

It appears from TEM measurements (Fig. 8-a) that two kinds of catalytic CNT co-exist at 450°C: the first one corresponds to MWNT of small outer diameter (12-25 nm) and the second one is constituted of 100-200 nm external diameter carbon filaments. At 550°C, the population of low diameter MWNT (9-15 nm) is largely dominant, but several filaments are still present. At 650°C (Fig. 8-b), a selectivity towards MWNT close to 100% is reached. At

700 and 750°C, we have observed the presence of significant amount of encapsulated iron nanoparticles in the samples (Fig. 8-c). The encapsulation may be due to sintering of iron nanoparticles at high temperatures. It has also been reported, in the case of MWNT growth from ethane on Fe/Al<sub>2</sub>O<sub>3</sub> catalysts that, at high synthesis temperature the rate of carbon nucleation was too fast compared to that of precipitation resulting to a rapid encapsulation of the catalyst particles with a concomitant formation of carbon nanoparticles [20].

### Figure 8

The fact that at low temperatures, large diameter filaments are present and that these filaments are notably absent at higher temperatures should indicate that the formation of these two structures involves different mechanistic pathways. Indeed, these large diameter filaments grow on large catalyst particles, and the absence of these large particles at temperatures above 550°C indicates a restructuring of the catalyst at high temperatures. Metal dusting is a carburisation phenomenon, which occurs at 400–800 °C in strongly carburizing atmospheres [21], and this phenomenon could be at the origin of large particle disintegration into smaller ones at temperatures above 450-550°C. Iron particles fragmentation during carbon filaments growth was reported more than thirty years ago by Baker et al. [22]. As far as activation energies are concerned, for MWNT grown from iron and acetylene, values between 30-38 kcal/mol have been reported [23,24], whereas for large diameter carbon filaments also grown from iron and acetylene lower activation energies of 16 kcal/mol have been reported [25]. It is worth mentioning that these values are in the same range than the activation energy for carbon diffusion in  $\gamma$ -Fe (bcc-structure), 33.3-39.5 kcal/mol, and in  $\alpha$ -iron (bcc-structure), 10.5-16.5 kcal/mol. Thus we can propose that the large particles present at 450-550°C consists of  $\alpha$ -iron and gives large diameter carbon filaments. In that case the activation energy for filament

growth fits well with the activation energy for carbon diffusion in  $\alpha$ -iron. For small size nanoparticles (the diameter of nanoparticles present inside the MWNT ranged between 4 and 8 nm), either present at 450°C or produce by metal dusting at higher temperatures, it is possible that the transition of  $\alpha$ - to  $\gamma$ -iron occurs at lower temperature than in the iron-carbon system (723°C). On these small size nanoparticles, activation energy for MWNT growth fits well with the activation energy for carbon diffusion in  $\gamma$ -iron. The presence of  $\gamma$ -iron nanoparticles in have been recently reported [26-28] and size effects on the properties of nanomaterials, including size driven phase transition is a subject of growing interest [29,30]. Furthermore, below 550°C the temperature seems insufficient to allow a suitable decomposition of ethylene.

There also, samples corresponding to each run have been heated in air till 800°C so as to burn all carbon species, and the mean diameter of the resulting support has been measured by laser granulometry. The average diameter is equal to 108  $\mu\text{m}$  at 450°C, it reaches 50-55  $\mu\text{m}$  beyond 550°C whereas the average diameter of the catalytic support is of 110  $\mu\text{m}$ . We confirm that the explosion of alumina grains must be related to the formation of MWNT since this phenomenon remains very limited at 450°C and presents an equivalent intensity beyond this value. So at 450°C, only the iron nanoparticles located on the external part of the alumina grains are active for catalytic carbon deposition.

Finally, BET results relative to pure MWNT (alumina having previously been removed by acid treatments) are presented in Table 3, and the pore size distribution is given in Fig. 9. It can be observed that the specific surface area of pure MWNT increases significantly with growth temperature. MWNT produced at 650°C have a specific surface area of 190  $\text{m}^2/\text{g}$ , which is close to the data reported in the literature for MWNT produced by CVD methods (20-200  $\text{m}^2/\text{g}$ ) [20]. The porous volume is very low at 450°C and presents a constant value between 650 and 750°C. Moreover, at 700 and 750°C, a specific pore size distribution

appears, centered between 2.5 and 8.5 nm, in good agreement with the internal MWNT diameter. This trend is confirmed regarding the BJH adsorption and desorption diameters. These results mean that for temperature lower than 700°C, only the external porosity of MWNT is accessible, that means mainly the aggregated pores formed by the interaction of isolated MWNT. Recent results concerning benzene adsorption in MWNT have confirmed that the adsorption between the tubes is a very important effect [31]. Thus, for MWNT produced at 700 and 750°C, the internal porosity becomes accessible, thus leading to increased specific surface areas. This could mean that at these temperatures, MWNT present less structural defects, and in particular less graphene layers perpendicular to the nanotubes axis (bamboo like structure, see insert in Fig. 9). Various growth model for bamboo-like CNT (presence of compartments) have been proposed [32-35], based on different physico-chemical phenomena, including: i) cyclic changes of carbon supersaturation in the catalyst particle, ii) periodical melting of the catalyst particle or iii) differences in catalyst particle moving rate inside the MWNT and carbon growth rate. It is reasonable to assume that an increase in temperature growth may induces differences in the growth mechanism which will result in the formation of completely hollow structures. It is worth noting that the high surface area (454 m<sup>2</sup>/g) measured for MWNT grown at 750°C makes this material interesting for several key applications.

### **Table 3 and Figure 9**

#### **3.3. Influence of the total gas flow rate**

The influence of the initial fluidization ratio  $U/U_{mf}$  has been studied by modifying in equivalent proportion the three gas flow rates and run duration, so as to work with a constant amount of carbon introduced. For all these runs, the  $H_2/C_2H_4$  gaseous ratio has been kept

equal to the nominal value 75/25. These experiments, for which the initial fluidization ratio has been varied between 0.6 and 1.1 and the run duration between 107 and 192 min, correspond to R13 to R16 of Table 2.

The evolution of carbon yield, fixed bed height and MWNT formation rate with the initial  $U/U_{mf}$  ratio are given in Fig. 10. It appears that the carbon yield tends to increase when the  $U/U_{mf}$  ratio decreases for a similar amount of carbon introduced, certainly due to the fact that the residence time of the gaseous precursors into the bed increases. The results obtained for  $U/U_{mf} = 1$  and 0.87 are very similar, indicating that for this range of total gas flow rates, the process in this 5.3 cm reactor reaches some optimum conditions of run in terms of fluidization quality as in terms of MWNT formation.

### Figure 10

It is worth noting that the fluidized bed was partly agglomerated during run R16, i.e for  $U/U_{mf}$  equal to 0.62, which may have disturbed the results. We have already shown that MWNT formation produces 3D randomly oriented hanks mostly surrounding alumina particles. We have also observed that the mean diameter of alumina particles decreases when MWNT form. These two phenomena produce a bed of light particles whose fluidizability decreases with the amount of MWNT formed. Consequently, it is obvious that the lower the fluidization ratio, the less vigorous the mixing of powders due to gas flow will be, and the more important is the risk of agglomeration due to MWNT formation. Combined with an increased carbon conversion due to a higher residence time, this initial  $U/U_{mf}$  ratio equal to **0.62** seems to be the low limit in terms of total gas flow for the tested operating conditions in this equipment. Thus, this agglomeration phenomenon has certainly lowered the results obtained for run R16 in terms of carbon conversion and MWNT formation growth rate. It is



likely that in a fluidized bed reactor of higher diameter, with less wall effects, such agglomeration phenomena would not occur because the intrinsic fluidization quality would be better.

On the contrary, the MWNT formation rate tends to decrease with the fluidization ratio. For this series of experiments, the run duration is increased when the fluidization ratio is decreased. As we have seen that MWNT growth is important between 45 and 75 min of run, it is logic that longer experiments (here till 192 min) induce lower mean deposition rates.

The apparent densities of the final fixed bed of composite powder remain in the same order of magnitude than those previously measured, i.e.  $60 \text{ kg/m}^3$ . The density obtained for run R16 is higher ( $100 \text{ kg/m}^3$ ), because agglomeration phenomena have occurred during this run, producing denser blocks of composite powders.

Finally, the granulometry analysis of the catalyst, once the MWNT have been burnt, has revealed no influence of the fluidization ratio on the final mean diameter of alumina grains. The values obtained are comprised between 35 and 55 microns. This result confirms that for run durations greater than 40 min, the explosion of alumina grains due to MWNT formation is no more occurring and reaches a plateau corresponding to catalysts particles of 40-50 microns. No significant difference in MWNT morphology between the samples was noticed by TEM.

### **3.4. Influence of the total pressure**

This study was performed for the nominal values of gas flow rates of run R14, and for a run duration of 120 minutes. The total pressure into the reactor was varied between 1 and 1.3 **bar**. The exact operating conditions tested correspond to runs R14, R17 and R18 of Table 2. It is worth noting that this increase in total pressure has lead to an enhancement of the gaseous residence time into the bed since the fluidization ratio has been equal to 0.9 for run R17 and to

**0.77** for run R18. Additionally, the partial pressure of ethylene has been increased with this total pressure enhancement. The corresponding experimental results are given in Table 4.

**Table 4**

It clearly appears that an increase in the total pressure does not bring any advantage: the carbon yield, MWNT weight and MWNT formation rate are lower when the total pressure is increased, despite the concomitant enhancements of gas residence time and ethylene partial pressure. Formation of agglomerates was observed during run R18, certainly due to a too low fluidization ratio and this may have distorted results. But this negative influence of the total pressure could be explained by the fact that the limiting step of the process corresponds to mass diffusion into the meso- and micro-pores of our alumina grains or through the product nanotube mat that covers the catalyst.

. According to the kinetic theory of gases, our process is governed by two regimes of gas flow into the pores:

- 1) in the largest ones, the regime is intermediary, and the mass diffusivity of a gaseous mixture A and B can be quantified from the Chapman Enskog relation [36]:

$$D_{AB} = 1,8583 \cdot 10^{-7} \frac{\sqrt{T^3 \left( \frac{1}{M_A} + \frac{1}{M_B} \right)}}{P \sigma_{AB}^2 \Omega_D}$$

where P is the pressure in atm, T the temperature in K,  $M_A$  and  $M_B$  the molar masses,  $\sigma_{AB}$  and  $\Omega_D$  physical parameters characteristics of molecules. This relation shows that diffusivity decreases when pressure increases.

- 2) for the smallest pores, the regime is molecular (or discontinuous) and the diffusivity can be calculated, according to the kinetic theory of gases, by the Knudsen equation [37], which is pressure independent:

$$D = \frac{2}{3} r \sqrt{\frac{8RT}{\pi M}}$$

where  $r$  is the radius of the pores (m) and  $M$  the molar weight of the gas (kg/mol).

So, for the largest pores, if the total pressure is increased, the gas penetration into the pores will be lowered, and then the catalytic nanoparticles present near the grains core will be less active. This explanation has been confirmed by measurements of the mean diameter of alumina grains after the MWNT have been burnt. Indeed, as can be seen in Table 7, this mean diameter increases with the total pressure showing that gas penetration into the pores is less pronounced at high pressure. These results confirm that our process is limited by internal diffusion phenomena into the porosity of the catalysts or through the product nanotube mat that covers the catalyst. It can then be deduced that a lowering of the total pressure would be favorable to improve the catalytic efficiency of the process. A negative influence of an increase of the total pressure on MWNT yield has already been reported in the case of Fe/SiO<sub>2</sub> catalysts [38].

### **3.5. Influence of the C<sub>2</sub>H<sub>4</sub>/ H<sub>2</sub> ratio**

The C<sub>2</sub>H<sub>4</sub>/H<sub>2</sub> ratio has been varied between 0.11 and 0.66, through two distinct studies. In the first one, the ethylene percentage and run duration have been varied simultaneously so as to operate with a constant mass of introduced carbon. The second one has consisted in fixing the run duration at 120 minutes and in varying the ethylene concentration.

#### ***3.5.1. Constant mass of carbon introduced***

In this first study, the nitrogen flow rate has been fixed to 685 sccm, and the run duration, hydrogen and ethylene flow rates have been varied, as indicated in Table 2 (runs R19 to R21 and R14). During these runs, no agglomeration phenomenon has been observed. The

evolutions of carbon yield, final fixed bed height, MWNT formation rate and weight with the ethylene percentage are presented in Fig. 11.

### Figure 11

It can be observed that the carbon yield presents an optimum value for 25% of ethylene, the lowest values being obtained for 11 and 66%. The weight of MWNT increases with the ethylene percentage till 25% and becomes lower at 66% than at 10%. On the opposite, the MWNT formation rate linearly increases with ethylene concentration. This important result indicates that the corresponding kinetic law is positive order dependant of the ethylene partial pressure. It also shows that an increase in the ethylene partial pressure allows an enhancement of the MWNT formation rate without deactivation of the catalyst and without loss in selectivity. The final fixed bed height is around 35 cm at 10 and 20% of ethylene and exceeds 50 cm at 25 and 66%. These values result in apparent bed densities around  $97 \text{ kg/m}^3$  at 10-20%,  $61 \text{ kg/m}^3$  at 25% and  $66 \text{ kg/m}^3$  at 66%. So the more important the ethylene percentage is, the slighter is the density of the final bed till 25% of ethylene. The important value at 66% could explain the poor results obtained in terms of carbon yield and MWNT weight for run R21: they could be attributed to poor fluidization conditions and even to a beginning of partial bed agglomeration, induced by the important MWNT formation rate. The measurement of the granulometry distribution of alumina grains after the burning of MWNT has conducted to mean diameters close to 35-45 microns whatever the ethylene percentage. So, the explosion of catalytic grains due to MWNT formation is identical for all the ethylene percentages tested. Combined with the previous result, this could indicate that the hanks of MWNT are more numerous or MWNT are longer for the highest percentages of ethylene, i.e.

for the highest MWNT formation rates. Systematic TEM measurements have shown no influence of this parameter on the general morphology of MWNT.

### ***3.5.2. Variable mass of carbon introduced***

These experiments correspond to runs R22 to R24 and R14 of table 2. The carbon yield, the fixed bed height evolution, the MWNT formation rate and weight as a function of the ethylene percentage are given in Figure 12. It is worth noting that a partial agglomeration of the bed has occurred during run R23 (66% of ethylene), which may have distorted the corresponding results.

### **Figure 12**

It appears that carbon yield tends to decrease when ethylene partial pressure increases. This result seems logical since for an equivalent residence time of precursors into the bed and similar operating conditions, the carbon conversion will be higher for the lowest ethylene percentage. On the contrary, MWNT formation rate linearly increases with this ethylene percentage (except for the peculiar run R23). The CNT final weight logically presents a similar evolution. These results confirm that the kinetic law governing MWNT formation is positive order dependant on the ethylene partial pressure.

The final fixed bed height tends to increase with ethylene partial pressure. The bed density is comprised between 54 and 61 kg/m<sup>3</sup> for runs R23, R24 and R14 and is equal to 104 kg/m<sup>3</sup> for 11% of ethylene (run R22), due to the lower amount of MWNT formed. The measurement of granulometry distribution of alumina grains after the burning of MWNT has conducted to mean diameters close to 40-60 microns whatever the ethylene percentage. So the explosion of

catalytic grains due to MWNT formation is identical for all the ethylene percentages tested. There also, systematic TEM measurements have revealed no influence of the ethylene percentage on the general morphology of MWNT.

### **3.6. Product characterization**

An important aspect that should be taken into account when producing CNT on a large scale is the batch to batch reproducibility, and ability to supply consistent quality is becoming more of a challenge than mere quantity. Thus, we have taken care to characterize MWNT from three different batches grown at 650°C during 120 min (Table 5). As far as the purity of the as-produced material is concerned, analyses were performed by coupling TGA and TEM observations [5]: a selectivity towards MWNT formation close to 100% was measured. It could also be deducted from TGA analysis coupled with SEM/EDX analysis of the residue obtained after reacting the composite powders with air at 1000°C, that 3% of metal remains inside the MWNT produced. We have not measured significant variations in MWNT morphology or in other characteristics, pointing out the good reliability of our production process.

#### **Table 5**

### **4. Conclusions**

We have developed a selective fluidized bed CCVD process for large scale production of MWNT. We have studied the influence of run duration, temperature and gaseous phase on the CNT growth. The main conclusions that can be drawn from the present work are :

1. In the first stage of the process, MWNT growth induces an explosion of the catalytic grains, and the production of a composite powder consisting in MWNT hanks anchored to the catalyst grains. Then, further growth generates significant increases in fixed bed height and reductions in apparent density of the composite powders and in minimum fluidization velocity.
2. The temperature influences significantly the morphology of the CNT hanks as well as the porosimetry properties of the MWNT. MWNT presenting a large specific surface area ( $450 \text{ m}^2/\text{g}$ ) have been produced at  $750^\circ\text{C}$ . The effect of the other parameters on MWNT morphology is less pronounced.
3. If the forces exerted by the gas on particles (fluidization ratio or total gas flow rate) become lower than the interparticles forces, which seem to increase with the amount of MWNT formed, a partial bed agglomeration occurs.
4. An increase of the total pressure does not brought any interest in terms of process efficiency for the range of operating conditions tested. A limiting step in this process is the internal diffusion into the mesopores of alumina.
5. The kinetic law of MWNT formation is positive order dependant of ethylene partial pressure at ambient pressure.

**Acknowledgements** : Prof. Jean Pierre Couderc (LGC, Toulouse, France) is gratefully acknowledged for helpful discussion. Prof. Jean Durand (IEM, Montpellier, France) is acknowledged for his help with SEM-FEG observations. These investigations have been supported by ARKEMA, Agence Nationale de Valorisation de la Recherche and Conseil Régional de Midi-Pyrénées.

## References

- [1] [http://www.arkemagroup.com/arkema/GB/comm\\_presse/d\\_comm.cfm?ID=622&prov=RLDRFT&motrech=nanotubes](http://www.arkemagroup.com/arkema/GB/comm_presse/d_comm.cfm?ID=622&prov=RLDRFT&motrech=nanotubes)
- [2] <http://www.research.bayer.com/research-news/nanotubes/page4246.htm>
- [3] [http://www.thomas-swan.co.uk/pages/nano\\_home.html](http://www.thomas-swan.co.uk/pages/nano_home.html)
- [4] Monthieux M, Serp P, Flahaut E, Laurent C, Peigney A, Razafinimanana M, Bacsa W, Broto JM. Introduction to carbon nanotubes. In "Springer Handbook of Nanotechnology" B. Bhushan (ed.), Springer-Verlag, Heidelberg, Germany, 2004, pp 39-98.
- [5] Corrias M, Caussat B, Ayrat A, Durand J, Kihn Y, Kalck P, Serp P. Carbon nanotubes produced by fluidized bed catalytic CVD: first approach of the process. *Chem Eng Sc* 2003;58:4475-82.
- [6] Wang Y, Wei F, Luo G, Yu H, Gu G. The large-scale production of carbon nanotubes in a nano-agglomerate fluidized-bed reactor. *Chem Phys Lett* 2002;364:568-72.
- [7] Qian W, Wei F, Wang Z, Liu T, Liu H, Luo G, Xiang L. Production of carbon nanotubes in a packed bed and a fluidized bed. *AIChE J* 2003;49(3):619-25
- [8] Nijkamp M. Hydrogen storage using physisorption: modified carbon nanofibers and related materials. Dissertation PhD thesis, Utrecht 2002:23-41.
- [9] Qian W, Liu T, Wang Z, Wei F, Li Z, Luo G, Li Y. Production of hydrogen and carbon nanotubes from methane decomposition in a two-stage fluidized bed reactor. *Appl Catal A*: 2003;260(2):223-8.
- [10] Venegoni D, Serp P, Feurer R, Kihn Y, Vahlas C, Kalck P. Parametric study for the growth of carbon nanotubes by catalytic chemical vapor deposition in a fluidized bed reactor. *Carbon* 2002;40:1799-1807.



- [11] Pérez-Cabero M, Rodríguez-Ramos I, Guerrero-Ruiz A. Characterization of carbon nanotubes and carbon nanofibers prepared by decomposition of acetylene in a fluidized bed reactor. *J Catal* 2003; 215:305-16.
- [12] Wang Y, Wei F, Gu G, Yu H. Agglomerated carbon nanotubes and its mass production in a fluidized-bed reactor. *Physica B* 2003;323:327-9.
- [13] Mauron P, Emmenegger C, Sudan P, Wenger P, Rentsch S, Züttel A. Fluidized bed CVD synthesis of carbon nanotubes on Fe<sub>2</sub>O<sub>3</sub>/MgO. *Diamond Rel Mater* 2003;12:780-5.
- [14] Bachilo SM, Balzano L, Herrera JE, Pompeo F, Resasco DE, Weisman RB. Narrow (n,m) distribution of single-walled carbon nanotubes grown using a solid supported catalyst. *J Am Chem Soc* 2003;125:11186-7.
- [15] Li YL, Kinloch IA, Shaffer MSP, Geng J, Johnson B, Windle AH. Synthesis of single-walled carbon nanotubes by a fluidized-bed method. *Chem Phys Lett* 2004;384:98-102.
- [16] Liu QX, Fang Y. New technique of synthesizing single-walled carbon nanotubes from ethanol using fluidized-bed over Fe-Mo/MgO catalyst. *Spectrochimica Acta A* 2006;64:296-300.
- [17] Serp P, Kalck P, Feurer R, Vahlas C. Method for the selective production of ordered carbon nanotubes in a fluidised bed. WO 2003/002456.
- [18] Hernadi K, Fonseca A, Nagy JB, Bernaerts D, Luca AA. Fe-catalyzed carbon nanotubes formations. *Carbon* 1996;34:1249-1257.
- [19] Do-Hyung K, Hoon-Sik J, Chang-Duk K, Dong-Soo C, Hee-Dong K, Jong-Gi J, Hyeong-Rag L. In situ monitoring of carbon nanotube growth. *Carbon* 2003;41:583-585.
- [20] Gulino G, Vieira R, Amadou J, Nguyen P, Ledoux MJ, Galvagno S, Centi G, Pham-Huu C. C<sub>2</sub>H<sub>6</sub> as an active carbon source for a large scale synthesis of carbon nanotubes by chemical vapour deposition. *Appl. Catal. A* 2005;279:89-97.

- [21] Lin CY, Tsai WT. Nano-sized carbon filament formation during metal dusting of stainless steel. *Mat. Chem. Phys.* 2003;82:929-936.
- [22] Baker RTK, Harris PS, Thomas RB, Waite RJ. Formation of filamentous carbon from iron, cobalt and chromium catalyzed decomposition of acetylene. *J. Catal.* 1973;30:86-95.
- [23] Liu K, Jiang K, Feng C, Chen Z, Fan S. A growth mark method for studying growth mechanism of carbon nanotube arrays. *Carbon* 2005;43:2850-2856.
- [24] Kim KE, Kim K-J, Jung WS, Bae SY, Park J, Choi J, Choo J. Investigation on the temperature-dependent growth rate of carbon nanotubes using chemical vapor deposition of ferrocene and acetylene. *Chem. Phys. Lett.* 2005;401:459-464.
- [25] Baker RTK, Chludzinski Jr JJ. Filamentous carbon growth on nickel-iron surfaces: the effect of various oxide additives. *J. Catal.* 1980;64:464-478.
- [26] Prados C, Crespo P, Gonzalez JM, Hernando A., Marco JF, Gancedo R, Grobert N, Terrones M, Walton RM, Kroto HW. Hysteresis shift in Fe-filled carbon nanotubes due to g-Fe. *Phys. Rev. B* 2002;65:113405.
- [27] Kim H, Sigmund W. Iron particles in carbon nanotubes. *Carbon* 2005 ;43 :1743-1748.
- [28] Kim H, Sigmund W. Iron nanoparticles in carbon nanotubes at various temperatures. *J. Cryst. Growth* 2005;276:594-605.
- [29] Roduner E. Size matters: why nanomaterials are different. *Chem. Soc. Rev.* 2006 advanced article.
- [30] Sun CQ. Size dependence of nanostructures: impact of bond order deficiency. *Progress in Solid State Chem.* 2006, in press.
- [31] Gauden PA, Terzyk AP, Rychlicki G, Kowalczyk P, Lota K, Raymundo-Pinero E, Frackowiak E, Béguin F. Thermodynamic properties of benzene adsorbed in activated carbons and multi-walled carbon nanotubes. *Chem. Phys. Lett.* 2006;421:409-414.

- [32] Wang YY, Tang GY, Koeck FAM, Brown B, Garguilo JM, Nemanich RJ. Experimental studies of the formation process and morphologies of carbon nanotubes with bamboo mode structures. *Diamond Relat. Mater.* 2004;13:1287-1291.
- [33] Zhang XX, Li ZQ, Wen GH, Fung KK, Chen J, Li Y. Microstructure and growth of bamboo-shaped carbon nanotubes. *Chem. Phys. Lett.* 2001;333:509-514.
- [34] Lu Y, Zhu Z, Su D, Wang D, Liu Z, Schlögl R. Formation of bamboo-shape carbon nanotubes by controlled rapid decomposition of picric ac. *Carbon* 2004;42:3199-3207.
- [35] Kuznetsov VL. Mechanism of carbon filaments and nanotubes formation on metal catalysts. In, *Nanoengineered Nanofibrous Materials : Proceedings of the NATO ASI on Nanoengineered and Nanofibrous Materials*. Guceri S, Gogotsi, YG, Kuznetsov V (Eds). Kluwer Academic Pub. 2004, 19-34.
- [36] Bird RB, Stewart WE, Lightfoot EN. *Transport phenomena*, Wiley Ed., NY, 1960.
- [37] Knudsen M. *The Kinetic theory of gases*. John Wiley and Sons, NY, 1932.
- [38] Li WZ, Wen JG, Tu Y, Ren ZF. Effect of gas pressure on the growth and structure of carbon nanotubes by chemical vapor deposition. *Appl. Phys. A* 2001;73:259-264.

## Figure captions

Fig. 1: Experimental set up

Figure 2: Evolution of porous volume with pore size distribution for 2.5%Fe/Al<sub>2</sub>O<sub>3</sub>

Fig. 2: Evolution with time of carbon conversion and fixed bed height

Fig. 3: Evolution with time of (a) carbon conversion and fixed bed height and (b) MWNT weight and growth rate

Fig. 4: Evolution with time of the catalytic support mean diameter after the formation of CNT

Fig. 5: SEM micrograph of exploded catalytic grains

Fig. 6: Evolution with temperature of (a) carbon yield and fixed bed height and (b) MWNT weight and formation rate

Fig. 7: SEM-FEG micrographs of MWNT formed at various temperatures: (a) 550°C, (b) 650°C, (c) 750°C

Fig. 8: TEM micrographs of material grown at (a) 450°C; (b) enlargement of the circle present on Fig. 8-a; (c) 650°C and (d) at 750°C

Fig. 9: Evolution of porous volume with pore size distribution at various temperatures

Figure 10: Evolution with  $U/U_{mf}$  of (a) carbon yield and fixed bed height, and (b) of MWNT formation rate

Fig. 11: Evolution with ethylene percentage of (a) carbon yield and fixed bed height; and (b) of MWNT weight and formation rate

Fig. 12: Evolution with ethylene percentage of (a) carbon yield and fixed bed height (variable weight of carbon introduced); and (b) of MWNT weight and formation rate (variable weight of carbon introduced)

### Table captions

Table 1: Summary of the conditions tested for the study of the influence of temperature and run duration

Table 2: Summary of the conditions tested for the study of the gaseous phase influence

Table 3: BET results for various synthesis temperatures

Table 4: Results on the influence of the total pressure

Table 5: Characterization of MWNT grown at 650°C for 120 min

Run	R1	R2	R3	R4	R5	R6	R7	R8	R9	R10	R11	R12
T (°C)				650				450	550	650	700	750
Run duration (min)	5	15	30	60	90	120	150			120		

Table 1: Summary of the conditions tested for the study of the influence of temperature and run duration

Run	R13	R14	R15	R16	R17	R18	R19	R20	R21	R22	R23	R24
Run duration (min)	107	120	137	192	120	120	302	152	51	120	120	120
N <sub>2</sub> flow rate (sccm)	771	685	600	428	685	685	685	685	685	685	685	685
C <sub>2</sub> H <sub>4</sub> flow rate (sccm)	455	405	354	253	405	405	161	320	640	160	640	320
H <sub>2</sub> flow rate (sccm)	1350	1200	1050	750	1200	1200	1444	1280	960	1440	960	1280
U/U <sub>mf</sub>	1.1	1	0.87	0.62	0.9	0.77	1	1	1	1	1	1
Total pressure (bar)	1	1	1	1	1.1	1.3	1	1	1	1	1	1

Table 2: Summary of the conditions tested for the study of the gaseous phase influence

	Purified CNT (T=450°C)	Purified CNT (T=650°C)	Purified CNT (T=700°C)	Purified CNT (T=750°C)
$S_{\text{BET}}$ (m <sup>2</sup> /g)	94.8	189.9	405.4	454.7
Porous volume (cm <sup>3</sup> /g)	0.24	0.8	0.85	0.84
$d_{\text{BJH ads}}$ (Å)	125.3	194.1	93	71.1
$d_{\text{BJH des}}$ (Å)	110.6	173.3	81.6	61.3

Table 3: BET results for various synthesis temperatures



Pressure (bar)	1	1.1	1.3
Carbon yield (%)	62.4	48.4	50
Fixed bed height (cm)	51	30	38
$m_{\text{NT}}$ (g)	30.1	23.5	24.3
$m_{\text{NT}}/m_{\text{CATA}}$	0.6	0.47	0.48
Formation rate ( $\text{g}_{\text{NT}}/\text{g}_{\text{Fe}}/\text{min}$ )	0.2	0.156	0.162
$d_{50}$ ( $\mu\text{m}$ ) after MWNT burning	53.3	70.6	82.8

Table 4: Results on the influence of the total pressure

<b>Purity</b>	<b>Average ext. diam (nm)</b>	<b>Average number of walls</b>	<b>S<sub>BET</sub> m<sup>2</sup>/g</b>	<b>Pore volume (cm<sup>3</sup>/g)</b>	<b>d<sub>002</sub> (nm)</b>	<b>Real density</b>	<b>Raman<sup>a</sup> G/D intensity</b>	<b>XPS<sup>b</sup> C/O</b>	<b>Conductivity (S/m)</b>
97%	15-17	13-15	180-190	0.80-0.89	0.341-0.342	1.9	1.15-1.25	98.5/1.5 99/1	0.97-1.1

<sup>a</sup> Ratio of the intensity of the G and D bands; <sup>b</sup> Carbon to oxygen surface atomic ratio

Table 5: Characterization of MWNT grown at 650°C for 120 min

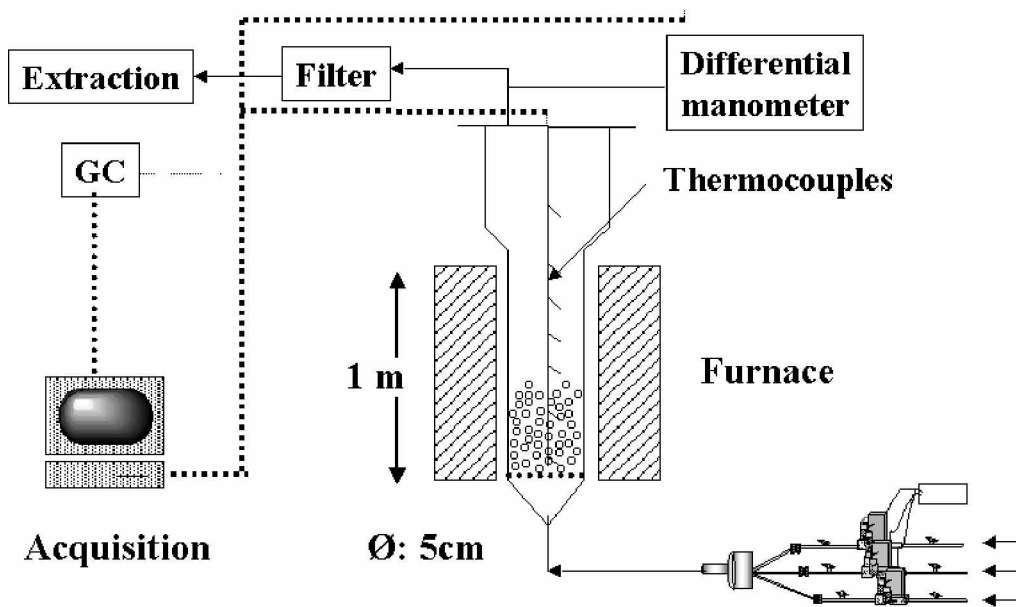


Fig. 1: Experimental set up

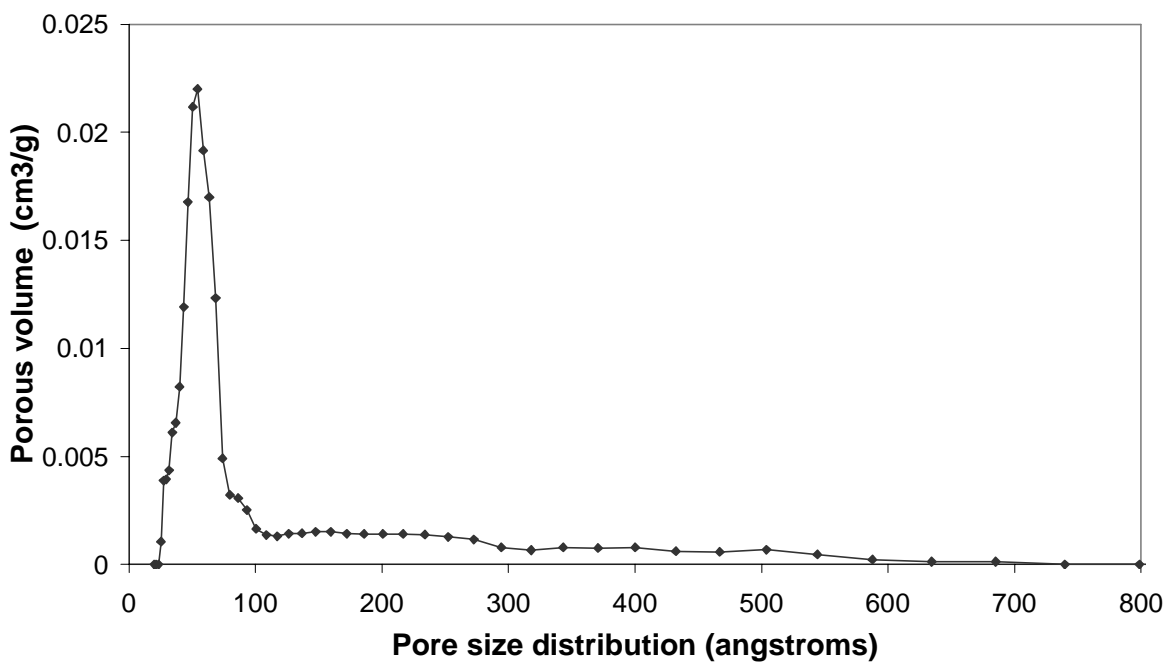


Figure 2: Evolution of porous volume with pore size distribution for 2.5%Fe/Al<sub>2</sub>O<sub>3</sub>

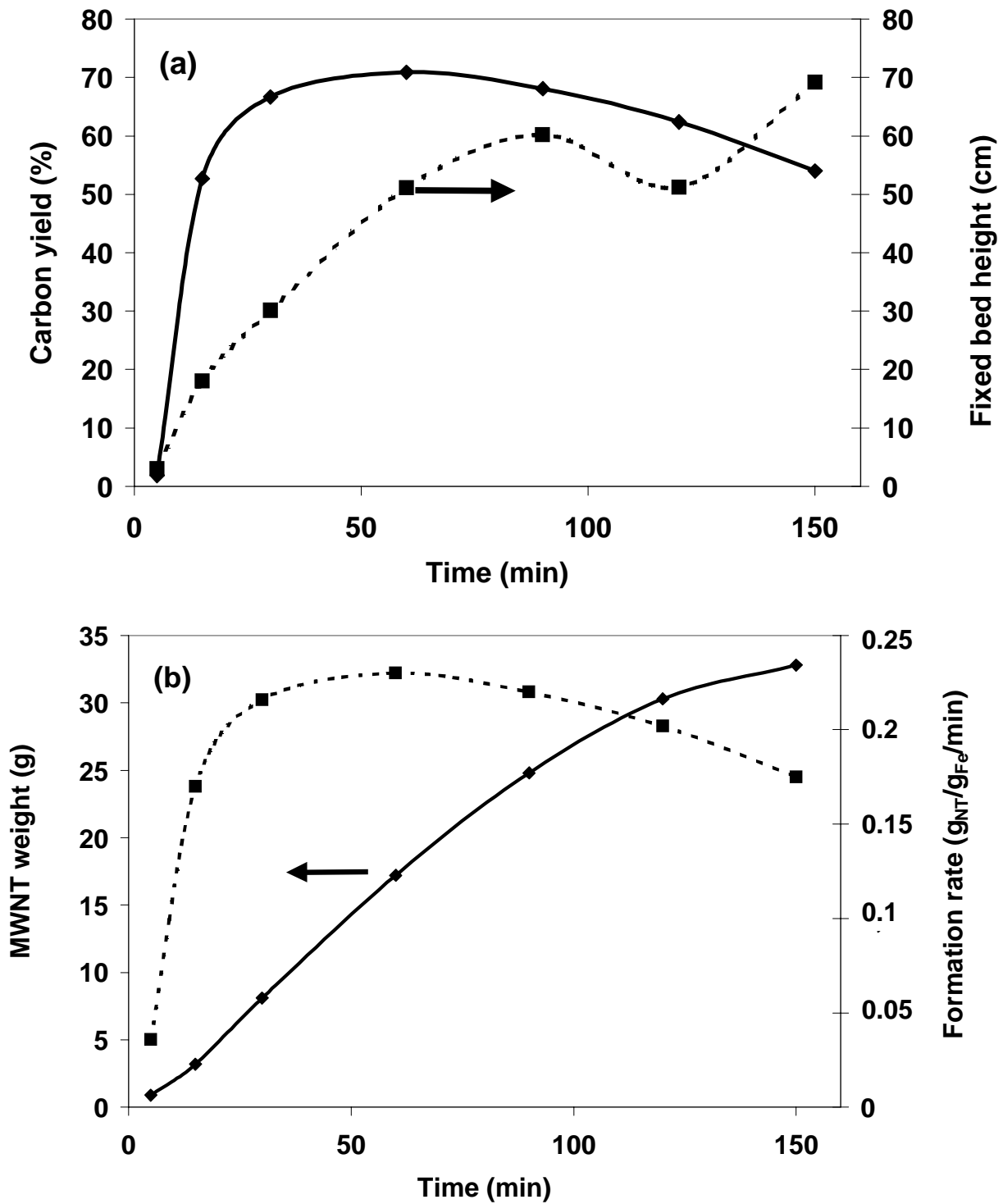


Fig. 3: Evolution with time of (a) carbon conversion and fixed bed height and (b) MWNT weight and growth rate

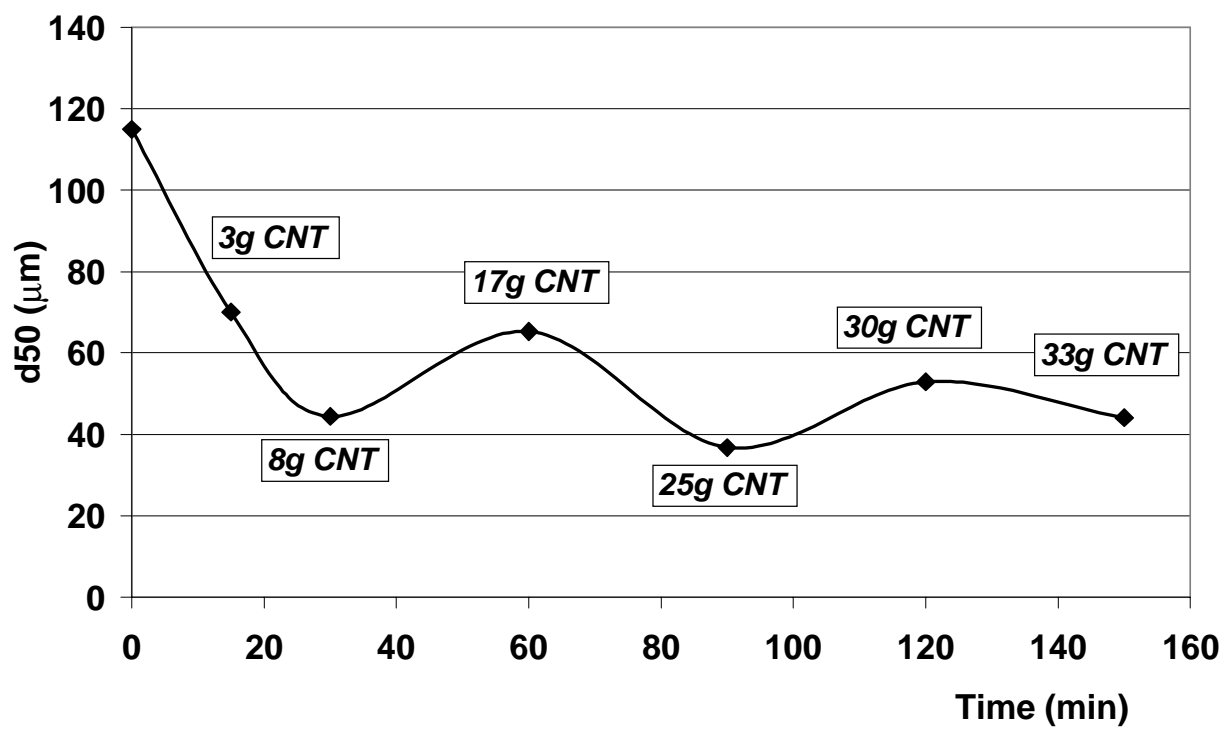


Fig. 4: Evolution with time of the catalytic support mean diameter after the formation of the nanotubes

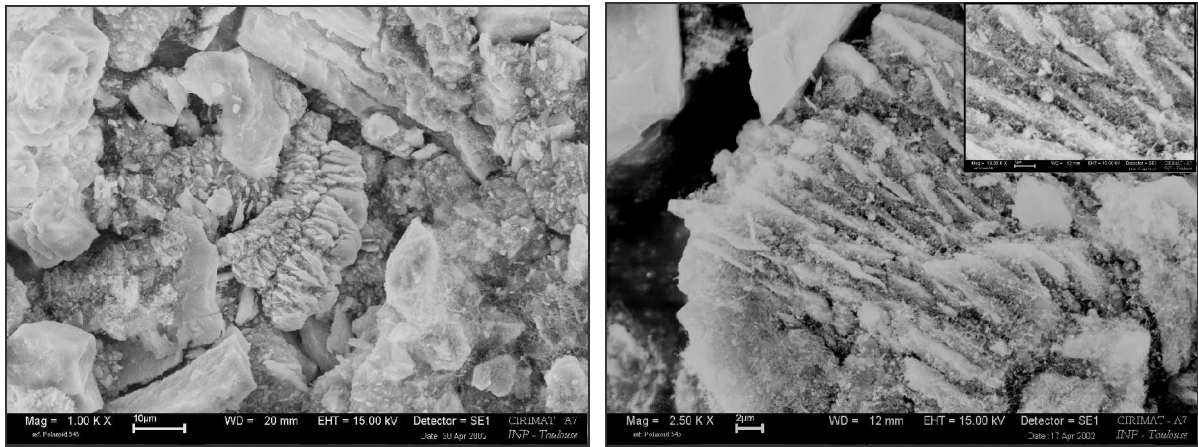


Fig. 5: SEM micrograph of exploded catalytic grains

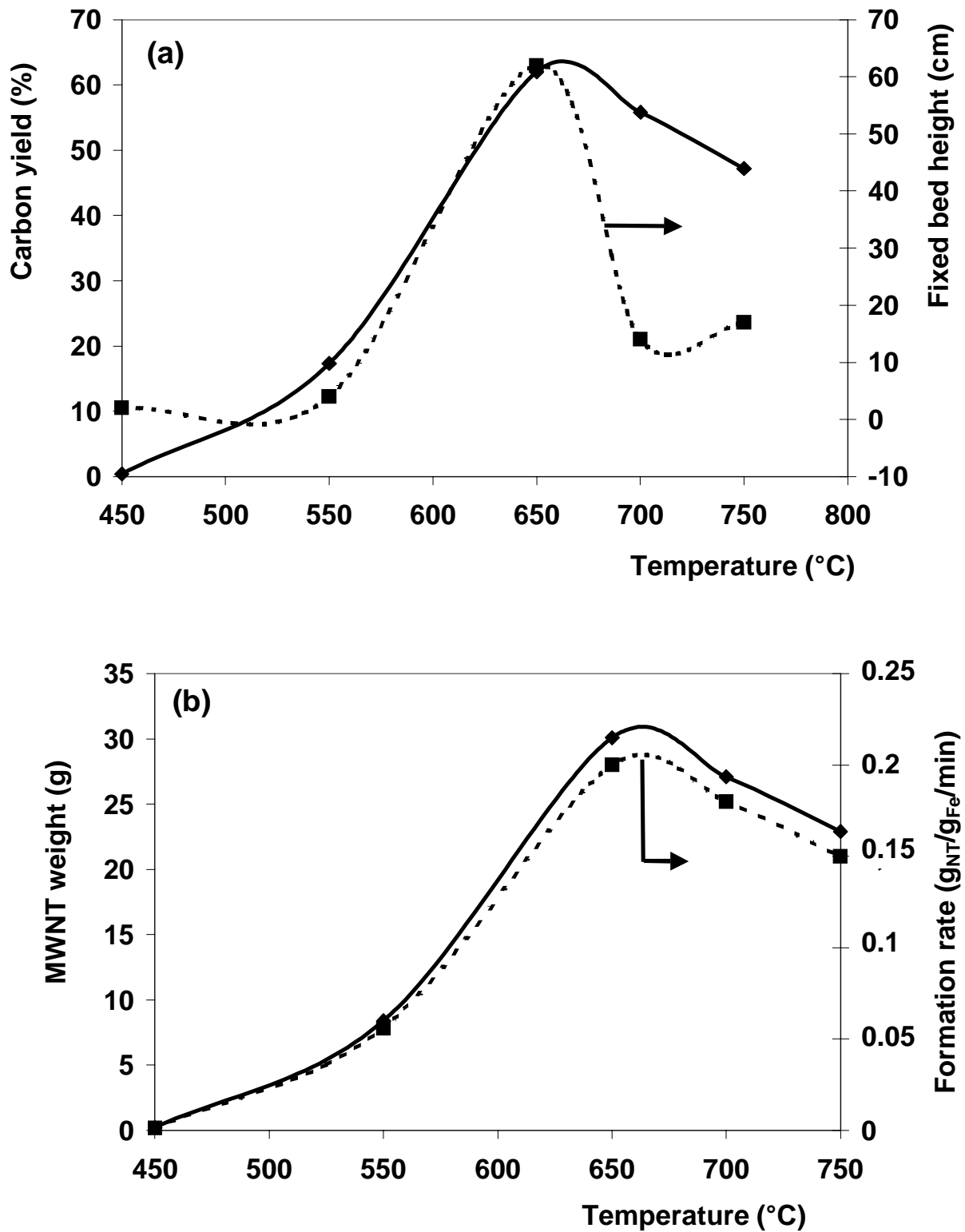


Fig. 6: Evolution with temperature of (a) carbon yield and fixed bed height and (b) MWNT weight and formation rate



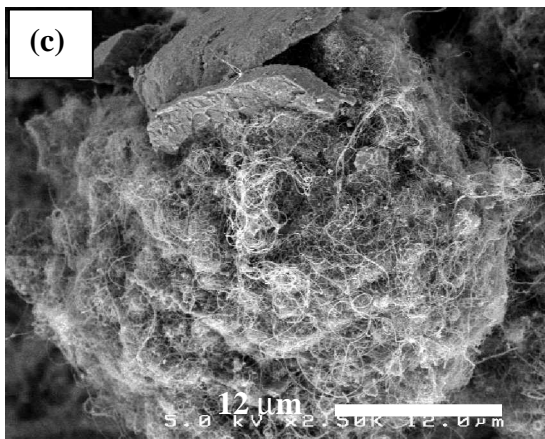
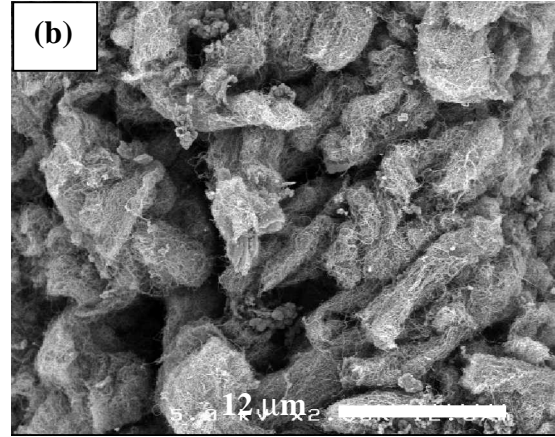
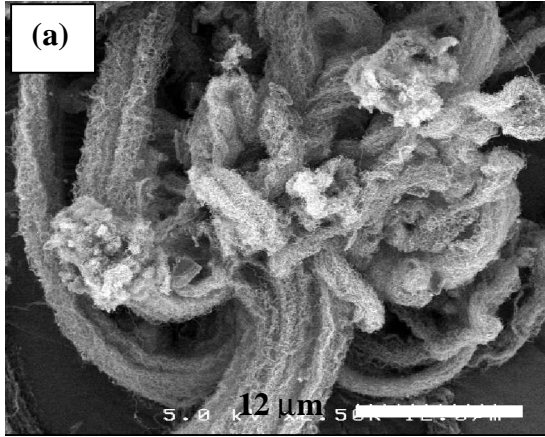


Fig. 7: SEM-FEG micrographs of MWNT at various temperatures: (a) 550°C, (b) 650°C and (c) 750°C

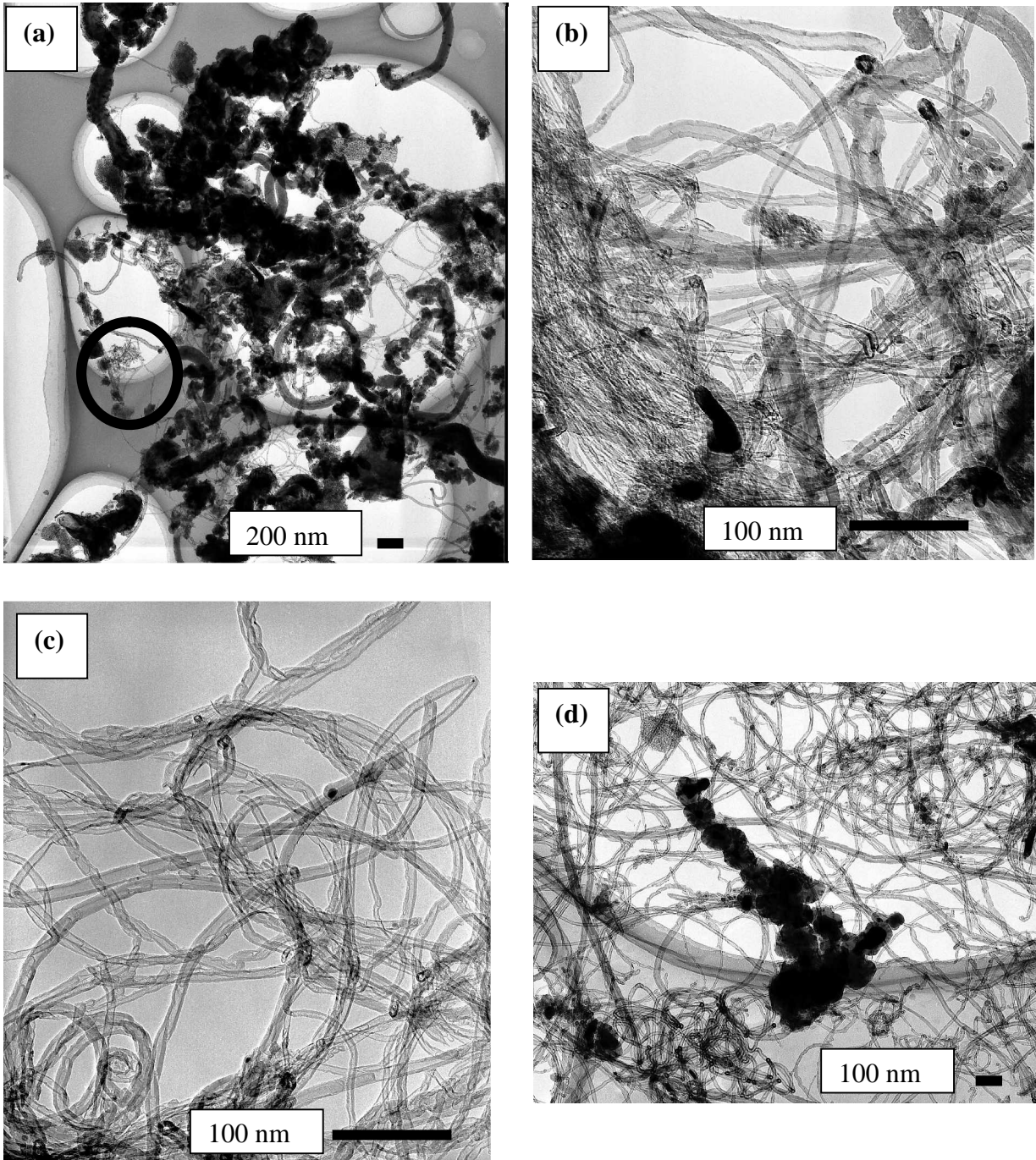


Fig. 8: TEM micrographs of material grows at (a) 450°C; (b) enlargement of the circle present on Fig. 8-a; (c) 650°C and (d) at 750°C

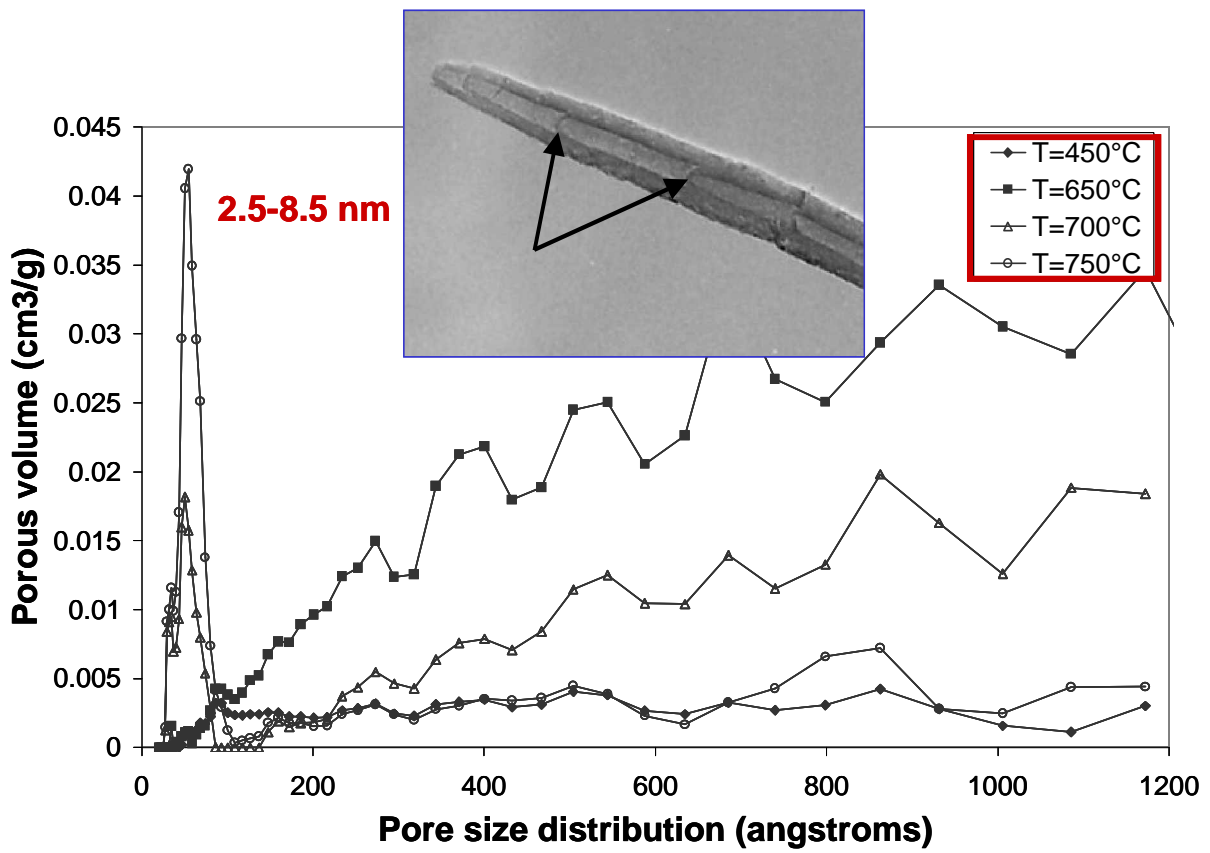


Fig. 9: Evolution of porous volume with pore size distribution at various temperatures. Insert: presence of defects (bamboo like structure in MWNT grown at 650°C).

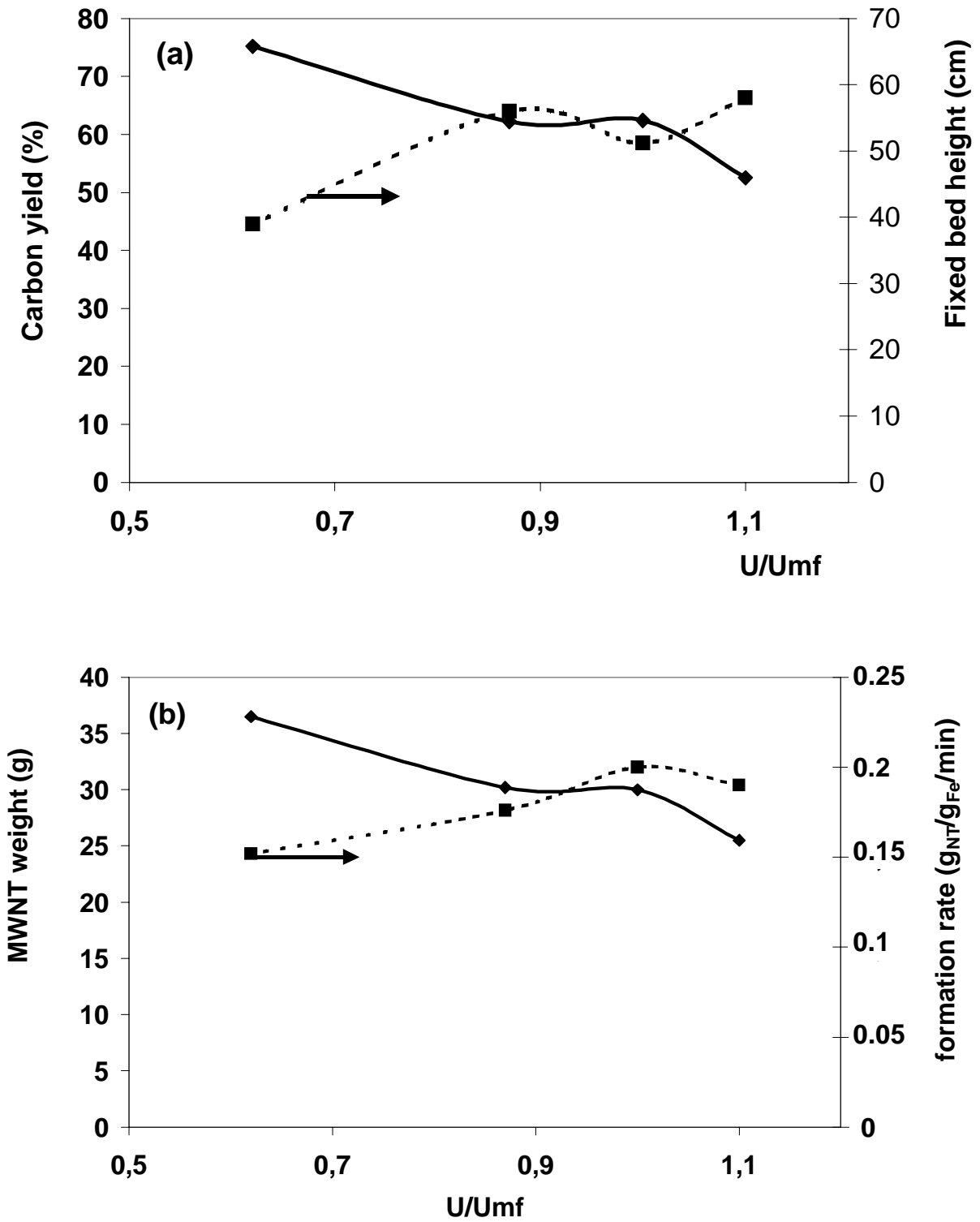


Figure 10: Evolution with  $U/U_{mf}$  of (a) carbon yield and fixed bed height, and (b) of MWNT formation rate

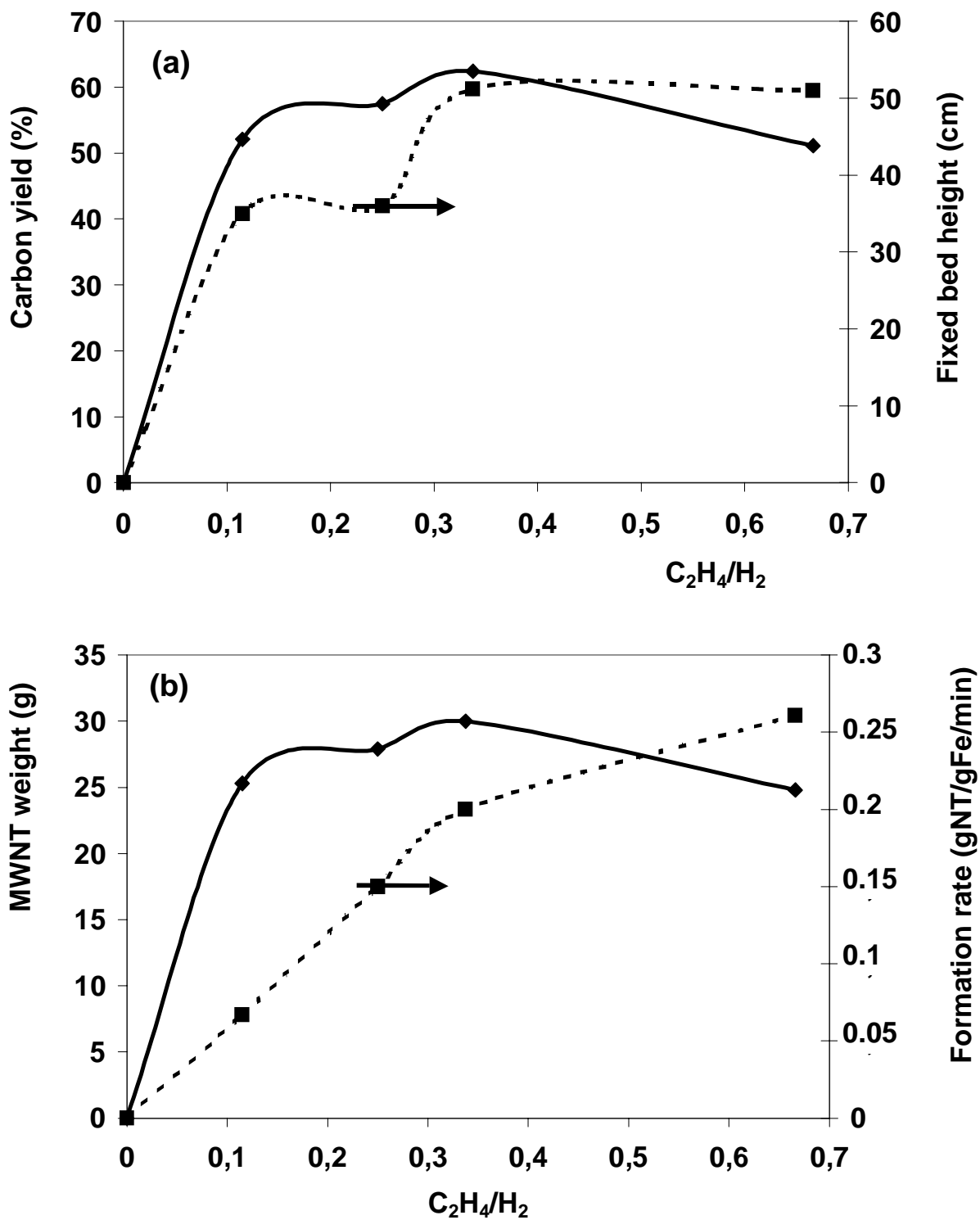


Figure 11: Evolution with ethylene percentage of (a) carbon yield and fixed bed height; and (b) of MWNT weight and formation rate

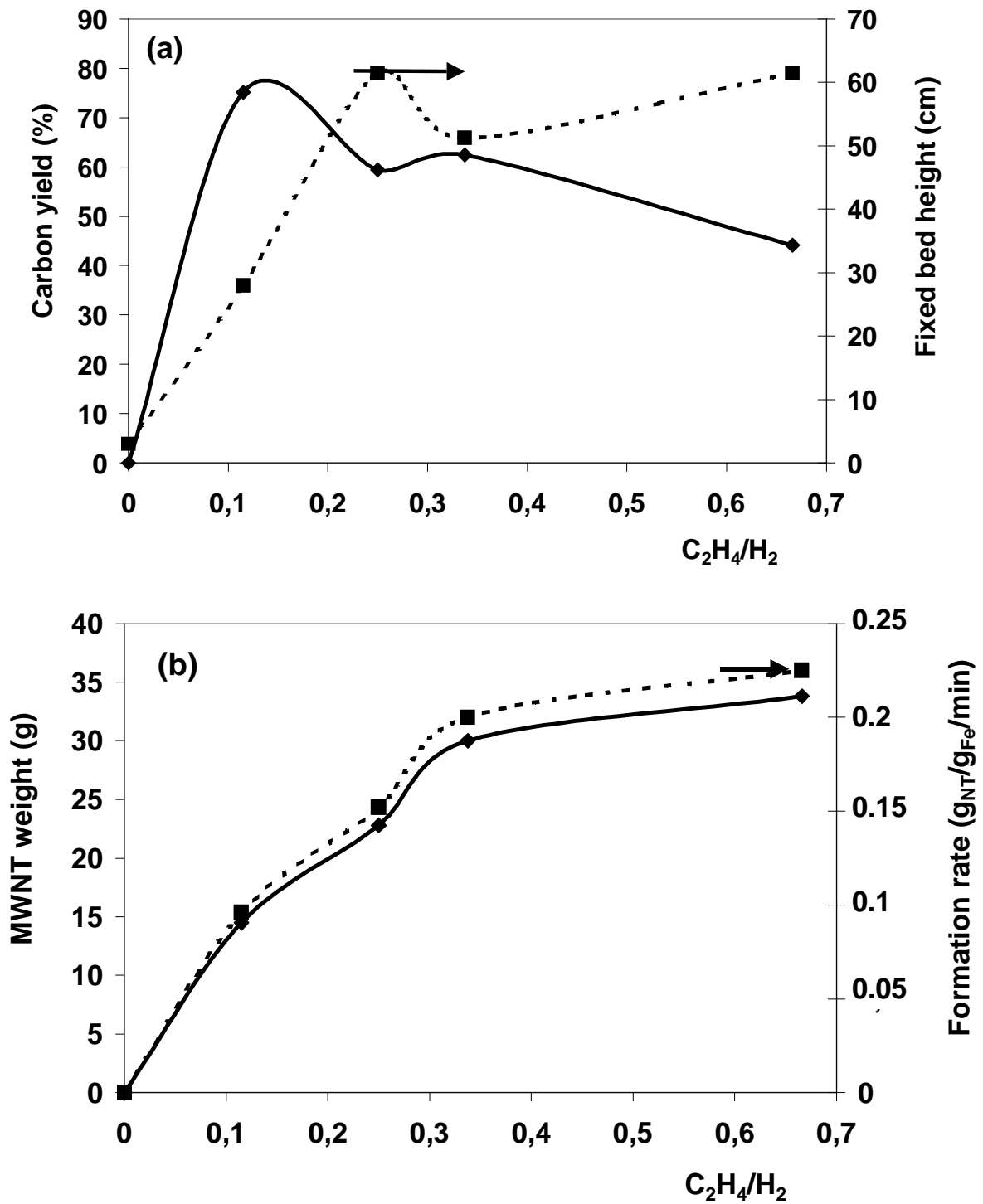


Figure 12: Evolution with ethylene percentage of (a) carbon yield and fixed bed height (variable weight of carbon introduced); and (b) of MWNT weight and formation rate (variable weight of carbon introduced)